Earth, Planets and Space

FULL PAPER Open Access

# Giant ionospheric density hole near the 2022 Hunga-Tonga volcanic eruption: multi-point satellite observations

Jong-Min Choi[1], Charles Chien-Hung Lin[1*], P. K. Rajesh[1], Jia-Ting Lin[1], Marty Chou[1], Young-Sil Kwak[2,3] and Shih-Ping Chen[1]

## Abstract

A giant ionospheric hole was simultaneously detected in the in situ measurements of FORMOSAT-7/COSMIC-2 (F7/C2), Ionospheric Connection Explorer (ICON), Swarm missions, and ground-based total electron content (TEC) by global navigation satellite system receivers, and F7/C2 Global Ionosphere Specification (GIS) data near Tonga, following the explosive volcano eruption on 15 January 2022. The TEC maps displayed the huge depletions that developed near Tonga after the eruption and gradually evolved. The ICON IVM, F7/C2 IVM and Swarm-LP detected large depletions not only near Tonga, but also in the EIA trough region. The GIS observations clearly show the ionospheric hole that extends spatially near Tonga, especially strongly south/southward. The simultaneous observations showed that the ionosphere hole near Tonga combined with the EIA trough and finally evolved into a giant ionosphere hole around 07 UT. The ionospheric hole, which occurred at 05 UT near Tonga, extended over a wide area of 160°-200°E and 25°S-20°N and lasted for about 11 h. The F7/C2 and ICON satellites overpasses showed large ion density depletions by the hole at orbit altitudes, accompanied by enhancements in ion temperature and field-aligned and perpendicular ion drift. Such a long-lasting giant ionospheric hole by a seismic event has not been reported earlier, creating a unique ionospheric environment near Tonga after the eruption. The strong successive impulses by multiple volcano eruptions, together with $O/N_2$ decrease in the summer hemisphere, interhemispheric wind, and water vapor injection into high altitudes apparently yielded such a giant ionospheric hole, 4–6 times larger than that observed during the Tohoku earthquake.

## Key points

1. The simultaneous measurements reveal the evolution of the ionospheric hole after the Tonga volcanic eruption.
2. The ionospheric hole that had occurred near Tonga merged with the EIA trough depletion in the northern hemisphere, forming a giant ionospheric hole.
3. The long-lasting giant ionospheric hole is caused by impulsive pressure, trans-equatorial wind, O/N2 depletion, and water vapor injection.

*Correspondence:
Charles Chien-Hung Lin
charles@mail.ncku.edu.tw
Full list of author information is available at the end of the article

**Keywords** Ionospheric hole, EIA trough depletion, Plasma transport, F7/C2 IVM, ICON, F7/C2 GIS

**Graphical Abstract**

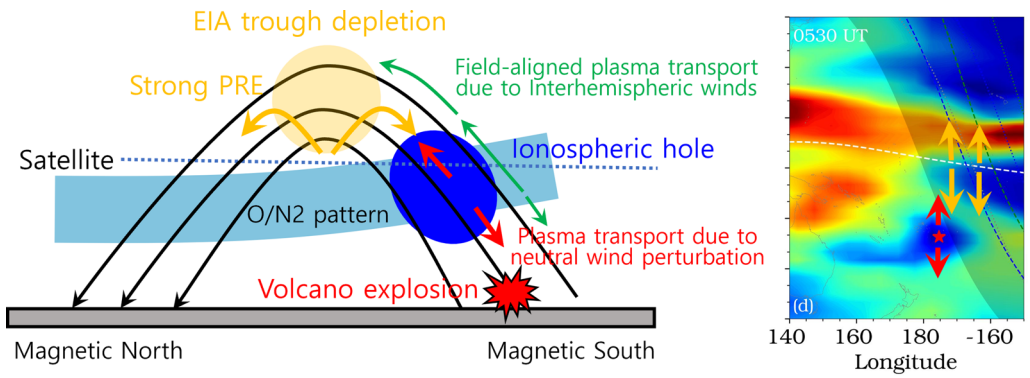


## Introduction

Natural hazards such as volcanic eruption, earthquake, and severe weather events generate acoustic and gravity waves that propagate vertically upward and cause significant perturbations in the ionosphere (e.g., Astafyeva and Afraimovich 2006; Astafyeva et al. 2019; Chou et al. 2017a; 2017b; Dautermann et al. 2009a; 2009b; Heki et al. 2006a, b; Liu et al. 1982, 2006a, b; 2010; 2011; 2016; Nakashima et al. 2016; Otsuka et al. 2006; Shinagawa et al. 2007; Shults et al. 2016; Sun et al. 2016). These ionospheric perturbations carry signatures of the generation and propagation characteristics of the atmospheric waves triggered after such events and enable further understanding of the atmosphere–ionosphere coupling and the associated electrodynamics. Apart from such perturbations, a noticeable decrease in total electron content (TEC) over a localized region near the epicenter, appearing as an "ionization hole", was reported following the M9.0 Tohoku earthquake of 11 March 2011 (Tsugawa et al. 2011; Saito et al. 2011; Kakinami et al. 2012; Astafyeva et al. 2013). The generation of the ionization hole has been reproduced by numerical simulations resulting from the nonlinear impacts of acoustic waves (Shinagawa et al. 2013; Zettergren et al. 2015, 2017; Zettergren and Snively 2019).

The recent eruption of the underwater volcano in Hunga Tonga-Hunga Ha'apai (hereafter Tonga) (184.6°E, 20.54°S) around 04:10 UT on 15 January 2022 produced unprecedented perturbations throughout the atmosphere (Adam 2022; Gusman and Rodger 2022; Wright et al. 2022). The ash plume penetrated the stratosphere and reached the mesosphere (altitude of 58 km) (Bates and Carlowicz 2022). The roar from this eruption was also heard in Alaska, 8000 km away from Tonga (Global Volcanism Program 2022). Several studies reported that the Tonga volcanic eruption caused significant atmospheric waves that propagated globally with the velocity of Lamb waves (Amores et al. 2022; Harding et al. 2022; Lin et al. 2022; Themens et al. 2022; Wright et al. 2022). Such studies examined the ionosphere variations from a global perspective, propagating to several thousands of kilometers from the eruption source. However, the Tonga eruption also produced large depletion in TEC measurements (Astafyeva et al. 2022), as reported following the Tohoku earthquake.

We investigate the evolution of a giant ionosphere hole after the eruption of the Tonga volcano, which persisted for ~ 11 h over a wide area of 160–200°E and 25°S–20°N by using ion-density measurements by FORMOSAT-7/COSMIC-2 (F7/C2), Ionospheric Connection Explorer (ICON), Swarm satellites, and F7/C2 Global Ionosphere Specification (GIS) electron density profiles constructed by assimilating radio occultation (RO) and global navigation satellite system (GNSS) slant TECs (Lin et al. 2017a, b; 2020), as well as TEC from ground-based GNSS network. A number of recent investigations reported the giant ionosphere hole in the low-latitude region near Tonga following the eruption (Aa et al. 2022; Astafyeva et al. 2022He et al., 2022). However, even in the equatorial region away from Tonga without ground GNSS receivers, the F7/C2, ICON, Swarm and F7/C2 GIS clearly observed large depletion in the EIA trough region. The ionospheric hole near Tonga evolved into the giant ionospheric hole with time as it was combined with the EIA trough. The space-based and ground-based data offer a unique opportunity to study ionospheric hole in

detail, with high spatial and temporal resolution. This paper focuses on observational evidence that ionospheric holes near Tonga are combined with large depletion in the EIA trough, and additional mechanisms for the formation of giant ionospheric holes. In Sect. "Instruments", we describe the data and instruments. The observation results are presented in Sect. "Results". In Sect. "Discussion", we discuss the characteristics of the ionospheric hole. Conclusions are given in Sect. "Conclusions".

## Instruments

The F7/C2 constellation consist of six satellites and was launched on 25 June 2019 by the Falcon Heavy of US Space Exploration Technologies Corporation (SpaceX) from the Kennedy Space Center in Florida, USA, on to a circular orbit at an altitude of ~ 700 km with 24° inclination angle. The Ion Velocity Meter (IVM) onboard F7/C2 measures in situ ion density, temperature, composition, and drift velocities in three directions with a data rate of 1 Hz (Heelis et al. 2017). The combination of six IVMs on each of the satellites provides the opportunity to study ionospheric events by in situ measurements with high spatial and temporal resolutions. In this study, satellite#1 of F7/C2 (simplified as F7/C2E1), F7/C2E3, and F7/C2E5 are used. In this paper we use the F7/C2 IVM Level 2 (ivmLv2) files. The ion density by F7/C2 IVM broadly agrees with orbit electron density by the Tri-GNSS radio occultation (RO) System (TGRS) (Chou et al. 2021; Chen et al. 2021). The IVM provides three-dimensional ion drift velocity for magnetic coordinates. Positive values indicate upward for the perpendicular drift and northward for the field-aligned drift, respectively. Since the calibration and validation of the F7/C2 IVM velocities are still underway, here we only examine the relative variation and direction of the velocities rather than the absolute values. In addition to the F7/C2 IVM ion density, the GIS electron density profiles constructed by assimilating RO and GNSS slant TECs (Lin et al. 2017a, b; 2020) are also used to examine the evolution and morphology of the ionosphere holes.

ICON was launched in October 2019 to an altitude near 580 km with an inclination angle of 27° (Immel et al. 2018). This study uses the ICON IVM measurements of the ion density and field-aligned ion velocity with 1 s time resolution. The ICON/IVM observations have been used to monitor ionospheric irregularities, which showed similar characteristics compared to the Ionospheric Plasma and Electrodynamics Instrument (IPEI) onboard ROCSAT-1 (Park et al. 2021) and Global-scale Observations of the Limb and Disk (GOLD), and Madrigal TEC measurements (Park et al. 2022a). The IVM onboard ICON is similar to those onboard F7/C2. In this study, we also use the electron density from the Langmuir Probes (LP) instrument onboard the Swarm-Charlie satellite. The Swarm-Charlie, one of the three satellites of the Swarm mission of the European Space Agency (e.g., Olsen et al. 2013; Lühr et al. 2015), has a circular polar orbit at an altitude of ~ 470 km with an inclination of 87.5°.

The GNSS TEC data from selected stations nearby Tonga are also used in this study. The 30-s sampled GNSS observations are used to derive vertical TEC at a sub-ionospheric altitude of 300 km, with a low elevation cut-off of 20° (Liu et al. 1996). A comparative study of two-dimensional TEC maps and IVM density is used to investigate the evolution of the ionosphere hole. In this paper, we use hourly median TEC maps by binning the measurements over 1°×1° latitude/longitude grids due to the sparse spatial coverage near Tonga. The details about the various data sources are provided in the Open Research section.

To understand the influence of thermosphere background conditions on the generation of the long-lasting giant ionosphere hole, we used not only the measurements of the thermospheric O/N2 ratio but also thermospheric neutral density. The Thermosphere Ionosphere Mesosphere Energetics and Dynamics (TIMED) satellite is in a circular orbit at 625 km with an inclination of 74°. The Global Ultraviolet Imager (GUVI) instrument onboard TIMED satellite provides the thermospheric O/N2 column density ratio (Paxton et al. 1999; Paxton et al. 2004; Christensen et al. 2003). In this study, we use the O/N2 data in Level 3, which are given in IDL save file.

The Gravity Recovery and Climate Experiment Follow-On (GRACE-FO) mission, consisting of two spacecrafts, was launched on 22 May 2018 into a near-polar orbit (inclination of 89°) with an initial altitude of about 490 km. The GRACE-FO electron density is the averaged electron density over ~ 220 km, which is calculated by dividing the horizontal TEC between the two GRACE-FO satellites by the inter-spacecraft distance (~ 220 km): see also Xiong et al. (2010) and Lühr and Xiong (2010). The thermospheric neutral density is measured by an accelerometer onboard GRACE-FO (Kornfeld et al. 2019). We use the GRACE-FO data at the ESA official web site: DNS folder (file identifier: GF_OPER_DNS1ACC_2) for thermospheric neutral density and NE folder (file identifier: GF_OPER_NE__KBR_2F) for electron density.

## Results

Figure 1 shows a significant depletion of vertical TEC over six GNSS stations (NMEA, TUVA, USP1, SAMO, RAUL, CKIS) in selected Global Positioning System (GPS) satellites (pseudo-random noise (PRN) codes PRN#10,21,32) near Tonga during the volcanic eruption from 04:00 to 09:00 UT on 15 January 2022. In the left panel, the red star indicates the location of Tonga,

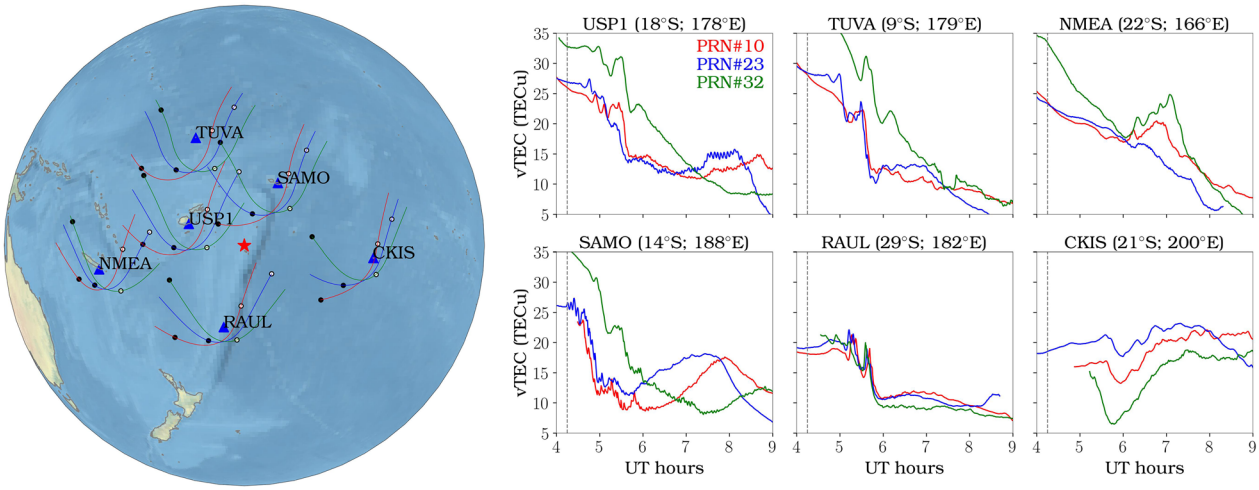


**Fig. 1** Times series of vertical TEC during Tonga volcanic eruption on 15 January 2022. (Left) The colored line and blue triangle indicate the trajectory of the ionospheric pierce point (IPP) during 4–9 UT and the location of GNSS station. The IPP are calculated assuming an ionospheric shell height of 300 km. The filled black and white circles on the trajectories indicate the beginning and end of the IPP location. The red star denotes the location of Tonga (184.6°E, 20.5°S). (Right) The variations of vertical TEC measured from six stations near Tonga for PRN#10(red), PRN#23(blue), and PRN#32(green). The black vertical dashed lines indicate the time of the 2022 Tonga volcanic eruption

and the blue triangles indicate the position of each station. The time series of TEC (right panels) exhibit a wave-like perturbation, with a sharp increase and then a large decrease. N-shaped TEC enhancement could be observed momentarily during the volcanic eruption. The onset time of the TEC enhancement depends on the distance between Tonga and the GNSS receiving stations. The stations closer to Tonga (TUVA, USP1, and RAUL) observed about three such enhancements between 5 and 6 UT, while stations relatively far from Tonga observed such enhancements after this period. Such TEC enhancements, related to the initial shock acoustic wave (Aa et al. 2022), are followed by large TEC depletions.

TEC in IPP trajectories close to Tonga (USP1, SAMO, TUVA, RAUL) decreased gradually from post-volcanic eruption to 6 UT, while TEC in the distant trajectories (NMEA, CKIS) decreased rapidly around 6 UT. In the CKIS station, the trajectory by CKIS-PRN32 passes through the region closer to Tonga compared to the others. The TEC variation shows a similar pattern for each satellite, but TEC by the CKIS-PRN32 is significantly reduced compared to CKIS-PRN10 and CKIS-PRN23.

Figures 2 and 3 show the temporal and spatial evolution of the huge plasma depletions near Tonga after the volcanic eruption: two-dimensional TEC maps (Figs. 2a–d, h–j, 3a–d, g–j), F7/C2 IVM and ICON IVM ion density (Figs. 2e–g, k–m, 3e, f, k–m), and Swarm-Charlie LP (Fig. 2n) between 0500 and 1900 UT on 15 January 2022. The magnetic coordinates are defined based on the quasi-dipole Apex coordinate system (Richmond 1995; Laundal and Richmond 2017). The black, blue, and green curved dashed lines represent the ground, E-region, and F-region sunset terminator location, and the grey dashed lines correspond to the night side. In the in situ measurements of satellites, the red vertical dotted line indicates the longitude position of Tonga. The TEC variation and plasma density over the longitude near Tonga are contrasted with the neighboring region of 140°E ~ 160°E and 200°E ~ 220°E. The location and local time of TEC depletion are consistent with those of in situ plasma density depletion measured by satellites. The nearly simultaneous and co-located observations of the F7/C2 IVM (~ 550 km altitude) and the ICON IVM (~ 600 km altitude) show nearly identical ion density depletion with each other (Fig. 2f).

The TEC map during 0400 ~ 0500 UT (Fig. 2a) shows the background ionosphere near Tonga before the eruption as a reference. No such decrease in the TEC distribution near Tonga was observed prior to the eruption (Fig. 2a) and on the previous day 14 January (Fig. 4). The huge plasma depletions observed on January 15, 2022 are thus associated with the Tonga volcanic eruption.

Figure 2b and 2e reveals the early stage of the depletion near Tonga after the eruption. The depletion caused by the eruption is almost identical to a rocket-induced ionospheric hole (e.g., Chou et al. 2018; Lin et al. 2017a, b; Park et al. 2022b). Since the ionospheric hole near Tonga appears in the observations even before sunset, it is unlikely to be the depletion signature of the equatorial plasma bubble, which generally occurs after sunset (e.g., Woodman 2009).

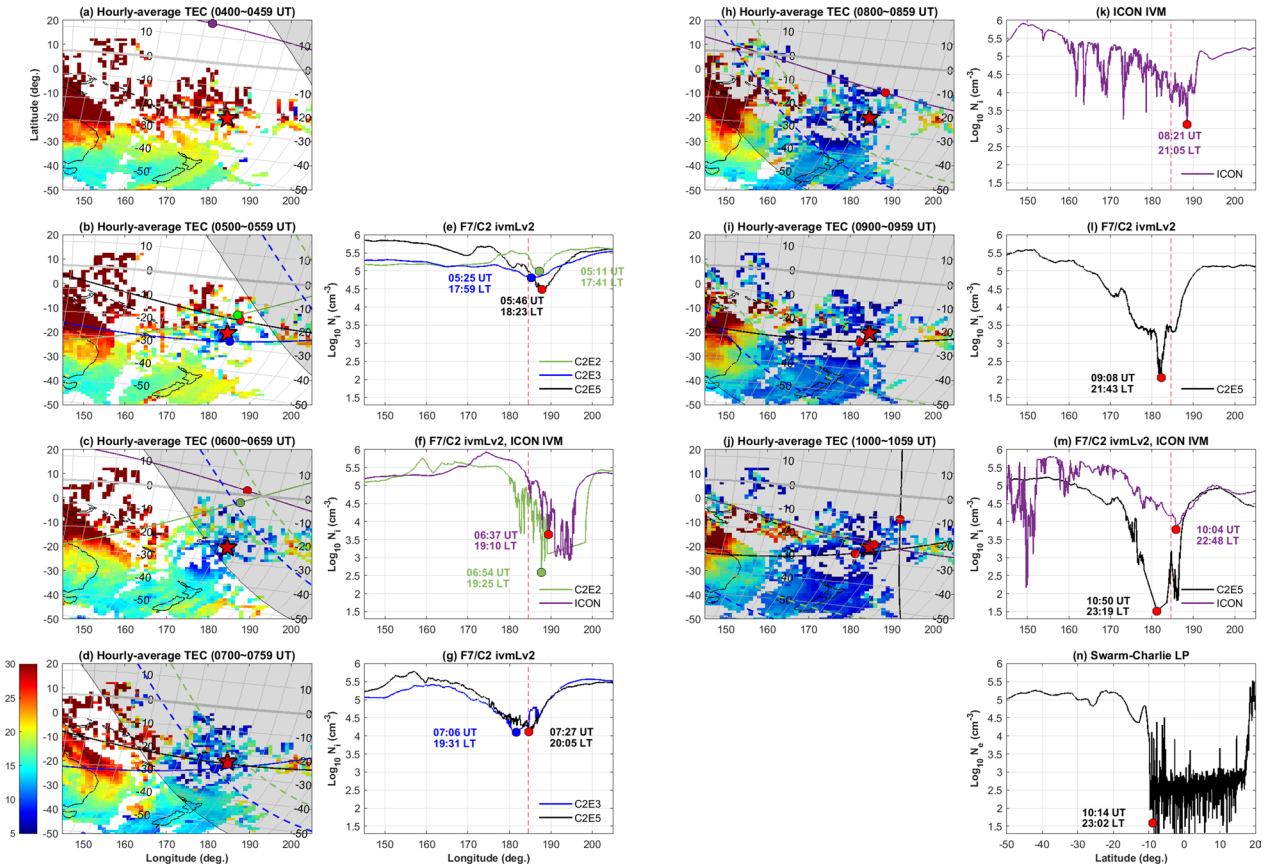


**Fig. 2** Evolution of the ionospheric hole by simultaneous measurements of the TEC map and F7/C2 IVM ion density during the Tonga volcanic eruption (04–11 UT). **a**–**d**, **h**–**j**) Satellite trajectory and (**e**–**g**, **k**–**n**) measurements of plasma density from F7/C2E2, C2E3, C2E5, ICON, and Swarm-Charlie are indicated by green/blue/black/purple/black horizontal lines, respectively. The curved dashed lines represent the ground (black), E-region (blue), and F-region (green) sunset terminator location, respectively, and grey area corresponds to the night side. The gray line and black numbers indicate the magnetic field line and magnetic latitude values, respectively. The star mark on the TEC map represents the location of the Tonga volcanic eruption. The color circles in satellite trajectory and plasma density indicate the location of minimum plasma density near the longitude of Tonga (180° ~ 190°E)

The TEC depletion showed that the ionospheric hole spatially expands near Tonga with time, especially strongly in the south/southward direction. Figure 5 shows the electron density at an altitude of 300 km during eruption obtained from the global ionosphere specifications (GIS).

Similar to the TEC map, the GIS electron density showed clearly the evolution of the ionospheric hole near Tonga on 15 January, extending in the south/southwestward direction (Fig. 5).

On January 15, in Fig. 5, the equatorial ionization anomaly (EIA) is identified by an electron density trough over the magnetic equator as well as two crests of enhanced electron density at about 15° north and south of the magnetic equator. The F7/C2 and ICON satellites not only observed the ionospheric hole near Tonga, but also observed a broad depletion with a zonal width greater than thousands of kilometers at the equatorial ionospheric anomaly (EIA) trough region (Fig. 2f and k). The EIA trough depletion gradually develops westward along the sunset terminator. The ionospheric hole near Tonga has a V-shaped structure with a minimum value in the vicinity of Tonga, whereas the EIA trough depletion has a relatively wider and deeper structure from the early stage after the eruption. The ionosphere hole near Tonga combined with the EIA trough depletion and finally evolved into a giant ionosphere hole around 07 UT. The ionospheric hole near Tonga also reached almost the same depth as the EIA trough depletion around 10 UT (C2E5 of Fig. 2m). Swarm-Charlie-LP observed the giant ionospheric hole formed from 10°S to 20°N (Fig. 2n). The giant ionospheric hole extended over a wide region of 160°-200°E and 25°S-20°N and lasted for about 11 h (05–16 UT).

The giant ionospheric hole is characterized by a large depletion reaching a minimum density of $\sim 10^{1.5} cm^{-3}$

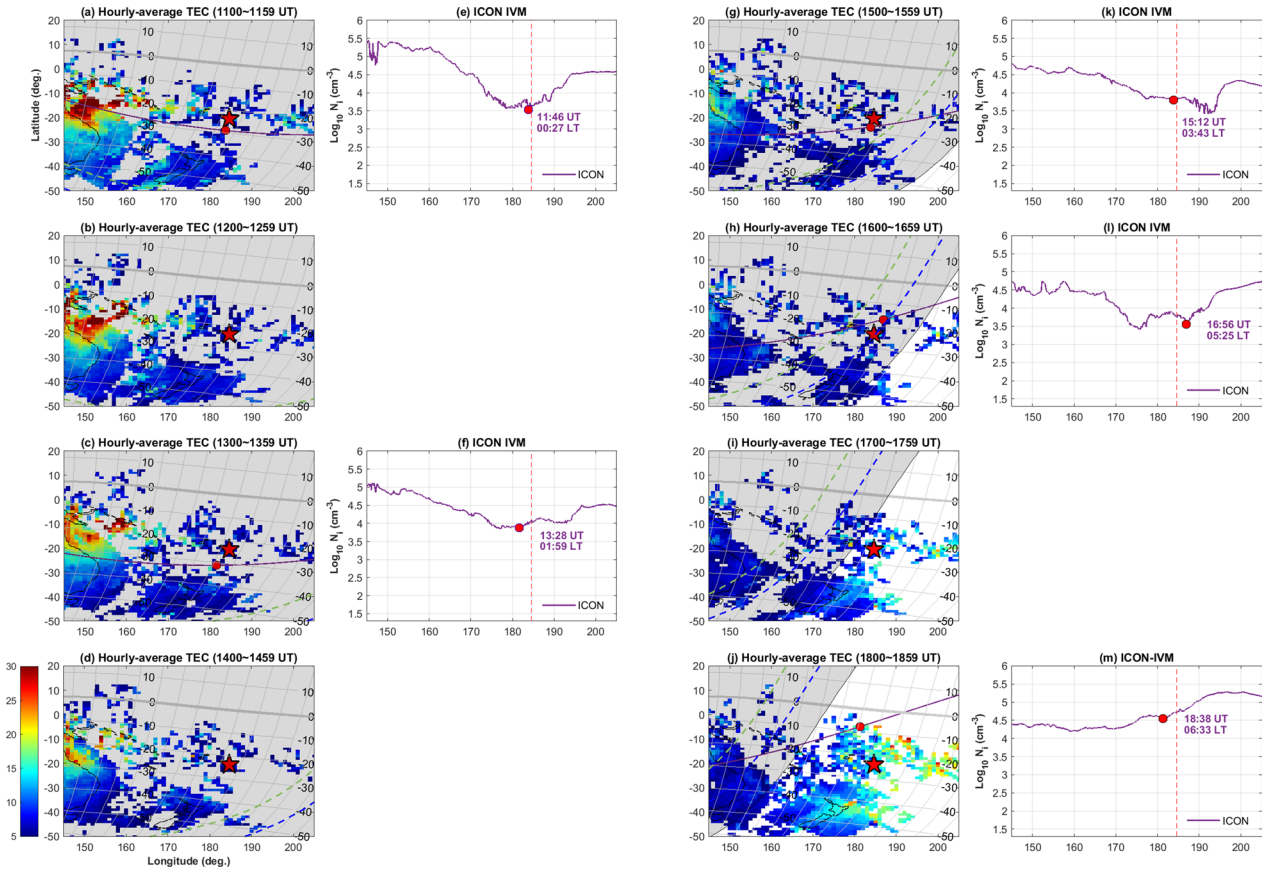


**Fig. 3** Same as Fig. 2 but for 11–19 UT

(Fig. 2m and 2n). The depth and duration of the giant ionospheric hole caused by the Tonga volcanic eruption are overwhelmingly larger than that of plasma depletion caused by other natural hazards. In Figs. 1 and 2, the TEC depletion depth (~10 TECu) by the Tonga volcanic eruption was significantly greater compared to the depletion depth by the Tohoku earthquake (~5 TECu) (Saito et al. 2011). The maximum density reduction at the ionospheric hole according to the in situ measurements is $\sim 4 \times 10^4 cm^{-3}$ (Fig. 2), which is significantly greater than the $\sim 2 \times 10^3 cm^{-3}$ reduction detected by ROCSAT-1 at an altitude of 600 km during the large magnetic storms of 29 October 2003 (Kil et al. 2006b, Fig. 4b). The ionospheric hole lasted for 11 h (05–16 UT) during Tonga volcanic eruption (Figs. 2 and 3), while the one in the Tohoku earthquake lasted for ~1 h. The giant ionospheric hole driven by the Tonga volcanic eruption has a longer time duration and stronger depletion effects on the ionosphere than other natural hazards.

Figure 6 presents the dynamic plasma conditions within the ionospheric hole near Tonga, depicting the plasma temperature and parallel and perpendicular drift observed by F7/C2 and ICON IVMs. In the first row, the blue lines represent the satellite trajectory, and the black dashed line depicts the magnetic equator. The black, blue, the green curved dashed lines indicate the sunset terminator in the ground, E-region, and F-region, respectively, and the grey shade region corresponds to night side. The orbits of F7/C2 and ICON satellites passed close to volcanic eruption while successfully performing in situ observation of ion density (second row), temperature (third row), field-aligned drift velocity (fourth row), and perpendicular drift velocity (fifth row). The giant ionospheric hole is detected with enhanced ion temperature and strong perturbations of field-aligned and perpendicular ion drift velocities near Tonga during a volcanic eruption. The ion temperature showed a substantial difference from the ambient temperature, reaching up to 4000 K. Near Tonga, overall field-aligned and perpendicular drifts are southward (i.e., poleward) and downward (i.e., toward lower L-shells), respectively.

The ion temperature enhancement at the ionospheric hole accompanied by poleward ion flow may be interpreted in the context of Su et al. (2003) and Huba et al. (2009). The two papers addressed ion temperature

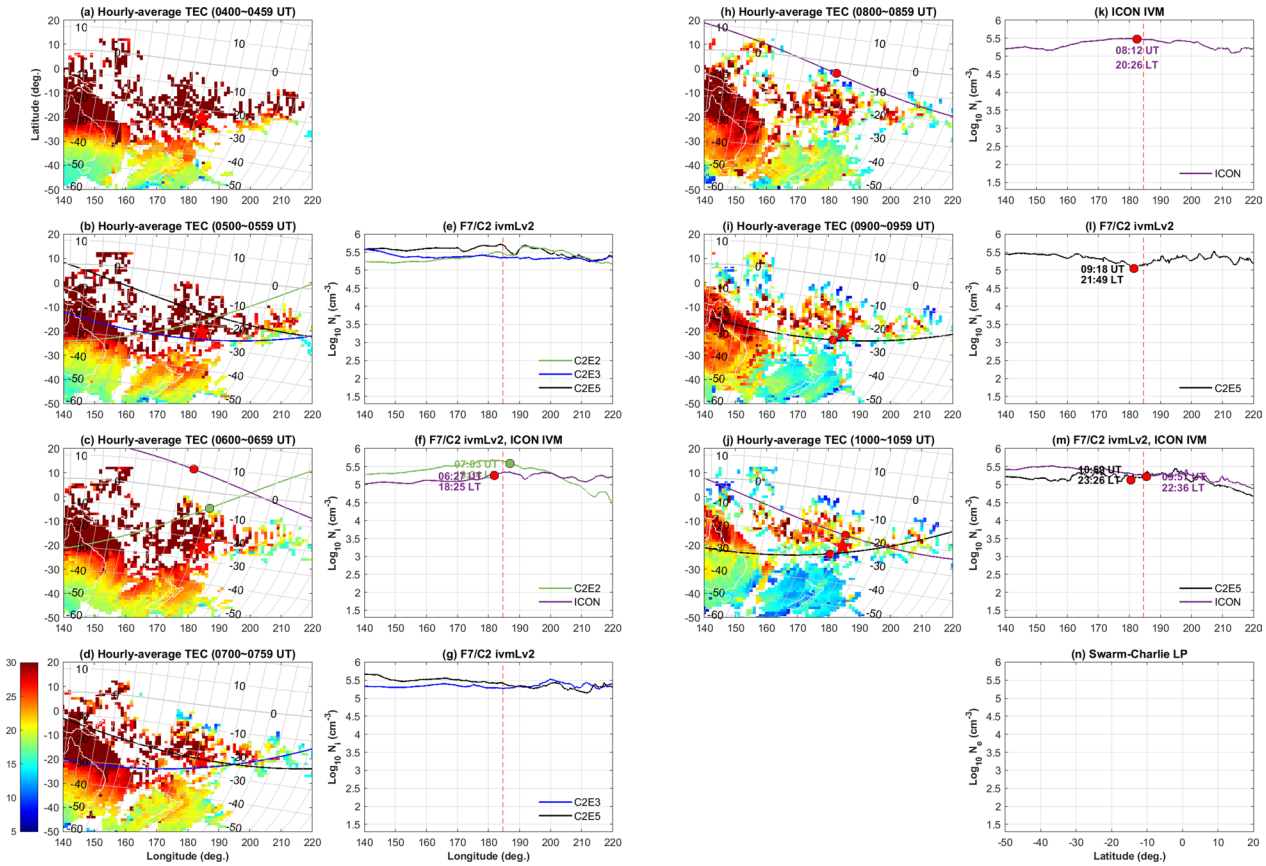


**Fig. 4** Same as Fig. 2 but on 14 January

enhancement inside density depletions using observations and simulations, respectively. Both suggested that field-aligned poleward transport of ions and concomitant compressional heating can lead to temperature enhancement. Huba et al. (2009) mentioned that ion temperature enhancement is affected by enhancement of large drift velocity due to ion-neutral frictional heating. Although the IVM drift velocity is not well calibrated, the fluctuating velocity of perpendicular drift is as large as 200 m/s. Such large perpendicular drift could also be a possible cause of the ion temperature enhancement through frictional heating.In Fig. 6a–d (05:11 UT), the longitude of minimum ion density corresponds to that of the maximum field-aligned drift velocity. However, the longitude of the maximum ion temperature is slightly westward, consistent with the longitude of the Tonga volcanic eruption. The longitude difference may be related to the strong impulse by the volcano eruption. This impulse not only affects the plasma temperature at an altitude of F7/C2 and ICON above the epicenter, but also pushes the plasma away from Tonga along the magnetic field line.

## Discussion

Using multiple point observations, we demonstrated that significant plasma depletion in the ionosphere is produced by Tonga volcanic eruption. The simultaneous observations of F7/C2, ICON, Swarm and TEC map show that the ionospheric hole near Tonga evolved into the giant ionospheric hole by combining itself with the EIA trough. Also, there are significant variations in ion temperature, and field-aligned and perpendicular drift near Tonga. Possible drivers that could result in the depletion are discussed as follows.

Shinagawa et al. (2013) performed a two-dimensional (altitude–latitude) simulation of the ionospheric hole occurring near the epicenter during the Tohoku earthquake. They find that a pressure bulge is created by the acoustic wave of the earthquake origin and leads to depletion. For the event presented here, the GRACE-FO satellite detects both the Tonga depletion and the equatorial trough (Fig. 7b), where the reduction of thermospheric neutral density also exhibited strong fluctuations (Fig. 7c). The impulsive bulge can cause localized divergence of the neutral wind and field-aligned ion motion, resulting in significant neutral and plasma

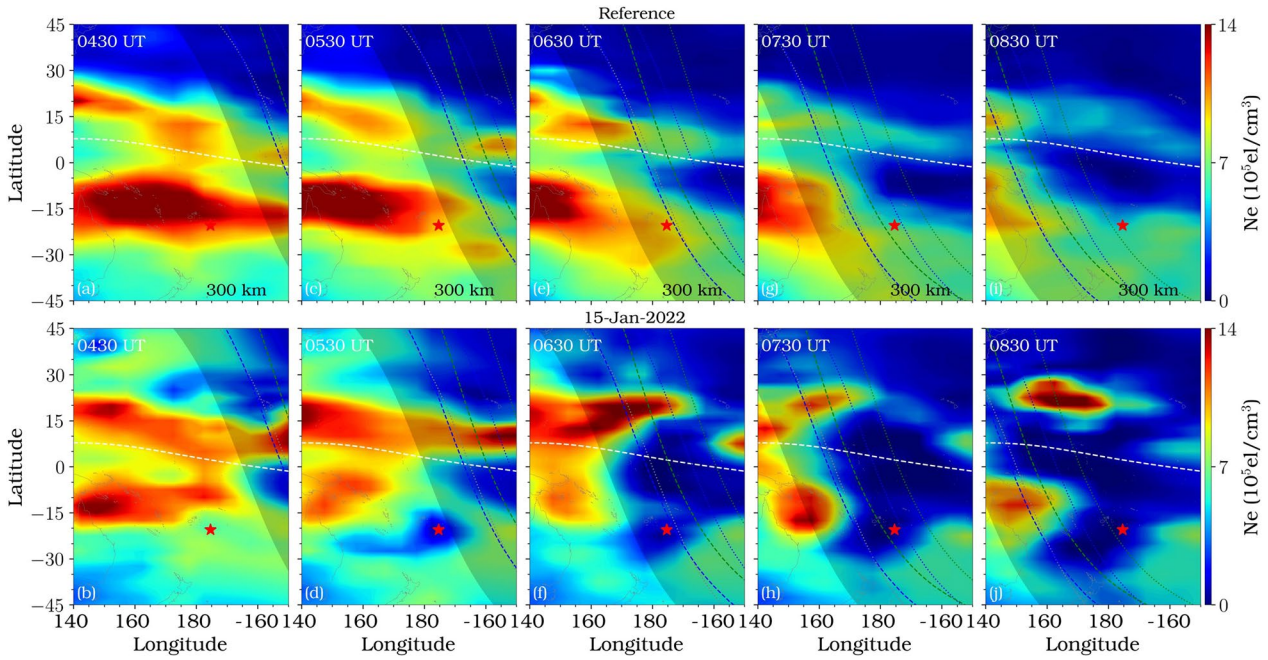


**Fig. 5** The longitude–latitude maps of electron density at an altitude of 300 km obtained from the F7/C2 GIS data during 0430–0830 UT, (**a**, **c**, **e**, **g**, **i**) the average electron density during the previous 5 days as reference. (**b**, **d**, **f**, **h**, **j**) the electron density on 15 January 2022. The white dotted line denotes the magnetic equator and the shaded region corresponds to the post-sunset period. The blue and green curves denote the sunset terminator in the E- and F-regions, respectively

density depletion above the epicenter. The schematic diagram in Fig. 8 illustrates the ionospheric hole around Tonga driven by the volcanic eruption according to this mechanism. The impulsive pressure pulse from volcanic eruption may have resulted in a significant expansion of the neutral atmosphere in the radial direction due to pressure gradient force, which drove the plasma along the magnetic field line away from the volcano. According to the simulation of Shinagawa et al. (2013), field-aligned plasma drift depends on the location of the eruption. The plasma motion is poleward/downward in the north of the epicenter and equatorward/upward in the south for the Tohoku earthquake in the northern hemisphere. Thus, the expected motion of plasma for the southern hemisphere is poleward/downward to the south of Tonga and equatorward/upward to its north (Fig. 8). At 05:11 UT in Fig. 6, the C2E2 trajectory moves from west to east as time progresses, showing a closer approach to the equatorial region. In the ionospheric hole near Tonga, the field-aligned plasma drift changes rapidly from southward to northward with latitude. The plasma drift predicted by Shinagawa et al (2013) seems to generally agree with the in situ measurements of plasma drift during Tonga volcanic eruption. However, the instantaneous northward drift within the strong southward drift at 07:27 UT, 10:03 UT, and 11:46 UT indicates that subtle differences also existed between actual observations and models for plasma drift around Tonga.

Saito et al. (2011) and Shinagawa et al. (2013) show that an ionospheric hole which occurred by the Tohoku earthquake only formed near the epicenter and expands in the radial direction. However, Zettergren et al (2017) reported a deeper ionospheric hole in the equatorial direction, due to the poleward/downward transport of plasma from equatorward to poleward. Kanai et al. (2022) improved the coverage of TEC data using Gaussian process regression and found that the TEC depletion extends more equatorward than poleward from the epicenter. On the other hand, Otsuka et al. (2006) discuss that the acoustic-gravity wave perturbations are more prominent in observations at the equatorward direction than poleward of epicenter due to that the wave fronts are aligned/perpendicular to the magnetic field line at equatorward/poleward direction. The mechanism is similar to that of Heki and Ping (2005). Shinagawa et al. (2007) suggest that at the equatorward of lower latitude, the magnetic field line is more horizontal and thereby the waves propagating along it experience the compression. However, at the poleward direction of the perturbation source, the magnetic field line has larger dip angle, and the ions are forced to lower altitude by neutral winds and lost more rapidly through ion-chemistry effects. The effect described by Shinagawa et al. (2007) fits our

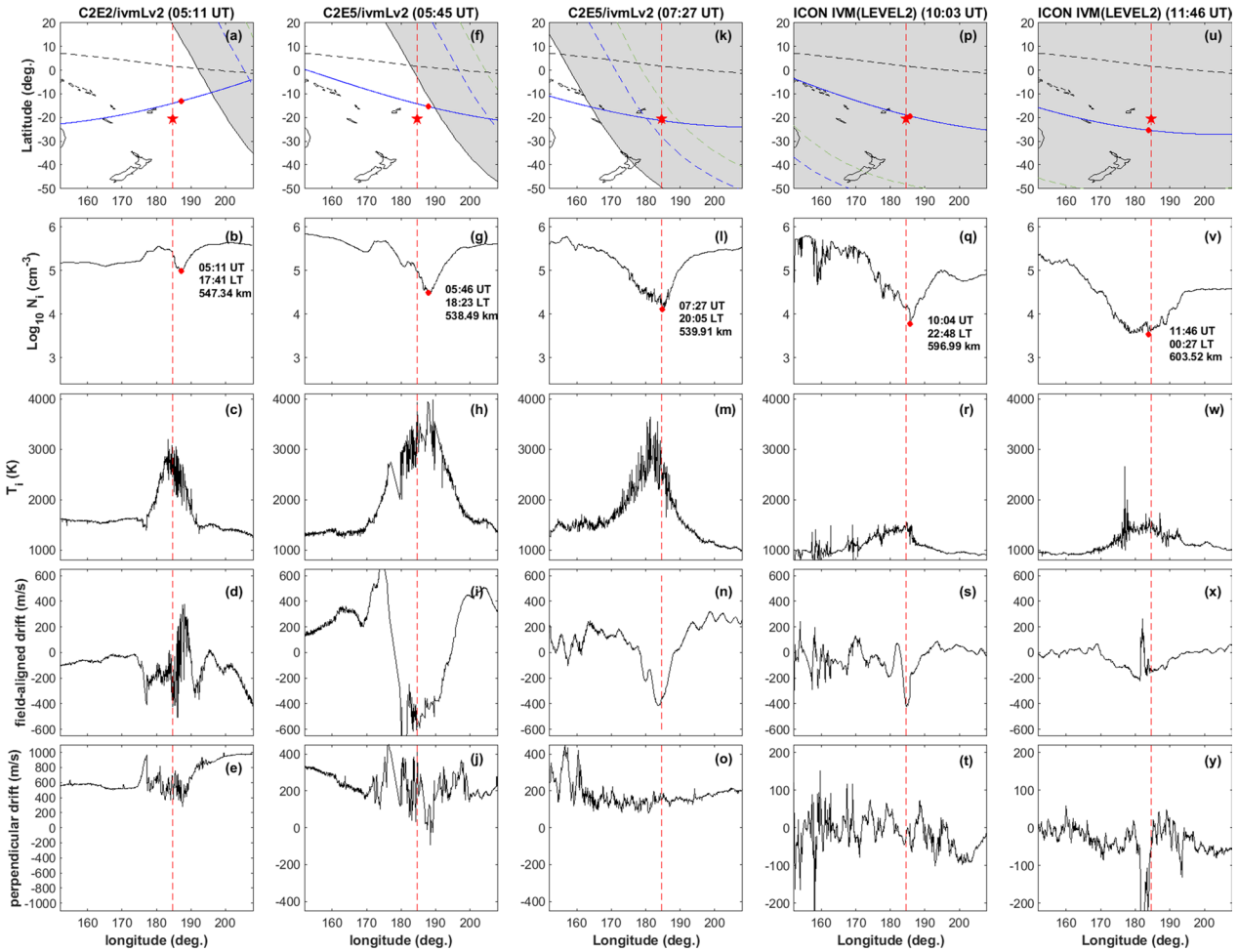


**Fig. 6** Detection of the ionospheric hole near Tonga measured by the F7/C2 and ICON satellites on 15 January 2022. From top to bottom panels are the F7/C2 satellite trajectory, the ion density, the ion temperature, and the parallel and perpendicular ion drifts, respectively. In the top panel, the black line is solar terminator, and the nightside is demarcated with grey shadow. The black dashed line indicates the magnetic equator. The star mark represents the location of the Tonga volcano and the red circles in satellite trajectory and plasma density indicate the location of minimum plasma density near the longitude of Tonga (180° ~ 190°E)

density hole observations better. The ionospheric hole near Tonga has evolved with a stronger spatial extension to the south/southwest rather than equatorward (Figs. 2 and 5), with the field-aligned drift after the volcano eruption being mostly poleward (Fig. 6). The strong poleward drift is also observed by C2E5 in the north of Tonga (Fig. 6f and 6i). The plasma around Tonga flew out poleward along the magnetic field line until at least 11:46 UT. The strong poleward plasma transport can influence the evolution of the ionospheric hole near Tonga, resulting in the south/southwestward expansion and deepening of the ionospheric hole in low latitude. Thus, the morphology of the Tonga ionosphere hole, which also lasted for a much longer duration, appears different from that during the Tohoku event.

The simulation model of the Tohoku earthquake needs to be supplemented to explain the much deepened and long-lasting ionospheric hole driven by the Tonga volcanic eruption. One possible factor is the strong successive impulses from volcanic eruptions. In Fig. 1, the TEC enhancement and depletion repeat at the SAMO station in the initial stage of the eruption, which means that the transport and recombination process by atmospheric expansion repeatedly affects the ionosphere. Aa et al. (2022) showed that acoustic wave impulses result in cascading TEC depletion. Astafyeva et al. (2022) reported five large explosions between 4 and 5 UT during the Tonga volcanic eruption. Repetitive neutral atmospheric expansion by successive volcanic eruptions may play an important role in the long-lasting ionospheric hole.

Additional factors that might have deepened the ionosphere hole could be the field-aligned plasma transport due to the interhemispheric wind (hereafter, interhemispheric wind) in the solstice conditions, and the seasonal

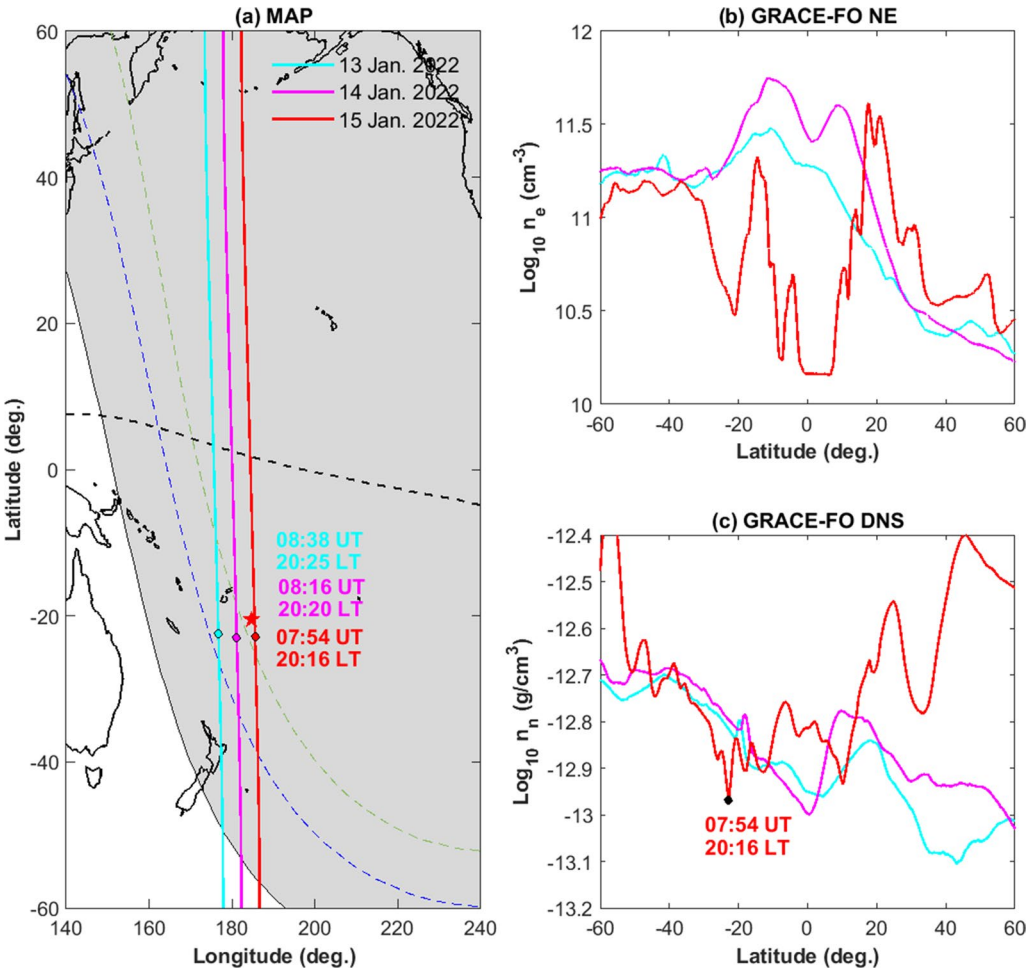


**Fig. 7** **a** Orbits of GRACE-FO on 13 (cyan), 14 (magenta), and 15 (red) January 2022. The red star indicates Tonga's location. **b** GRACE-FO measurements of the electron density along the orbits shown in **a**. **c** The neutral density depletion detected by accelerometer onboard GRACE-FO during Tonga volcano (red) as compared with the storm (green) and normal day (blue)

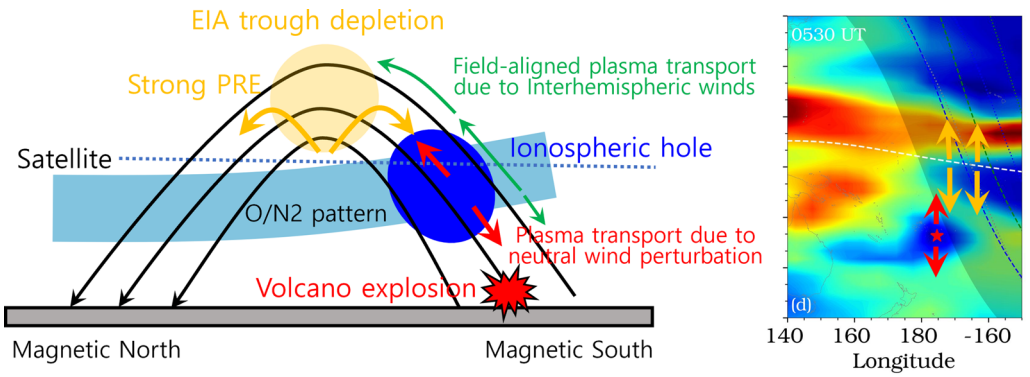


**Fig. 8** (Left) Schematic diagram of plasma motion during Tonga volcanic eruption based on the hypothesis proposed by Shinagawa et al. (2013). The ionospheric hole region and EIA trough depletion are indicated with blue and yellow shaded regions, respectively. The black lines show the magnetic field lines. The red lines denote the field-aligned plasma transport by neutral wind perturbations induced by the impulsive pressure pulse and the green arrows are those due to prevailing interhemispheric winds. The light-blue shade indicates the O/N2 pattern in the solstice. The plasma motion due to the strong PRE is indicated with yellow lines. (Right) Observation of electron density at 0530 UT (Fig. 5d). The yellow arrows denote the effects of enhanced PRE and the red arrows indicate the plasma motions caused by the impact of the volcano eruption

O/N2 pattern. In solstices, the interhemispheric wind generally transports plasma from the summer to the winter hemisphere. However, in the evening period when the volcano erupted, the interhemispheric wind in the summer hemisphere tends to be stronger equatorward from the latitude of Tonga, compared to middle and high latitudes (Lin 2005; Lin et al. 2012), as denoted by the green arrows in Fig. 8. This divergent meridional wind will transport plasma equatorward/upward from Tonga, further depleting the ionization there. The reduced O/N2 in the summer hemisphere due to upwelling (Fuller-Rowell et al. 1996), as sketched in Fig. 8, could further contribute to lowering the electron density above Tonga. Note that, the storm recovery conditions over this longitude in the evening sector following a geomagnetic storm had already weakened the electron density over the southern EIA latitudes (Rajesh et al. 2022).

Figure 9 shows the O/N2 ratio map from GUVI on 13–15 January 2020. The lower ratio in the longitude of 300–330°E and the latitude of 10°S–40°S is due to South Atlantic Anomaly (SAA). On 14 January, the O/N2 depletion extended further equatorward due to the impact of the geomagnetic storm, covering Australia. On January 15, the contrast of the O/N2 ratio between the southern and northern hemispheres was more pronounced. The reduced O/N2 ratio appeared near Tonga on 15 January 2022. It is interesting to note that the O/N2 ratio on the 14th was maintained over the Pacific Ocean

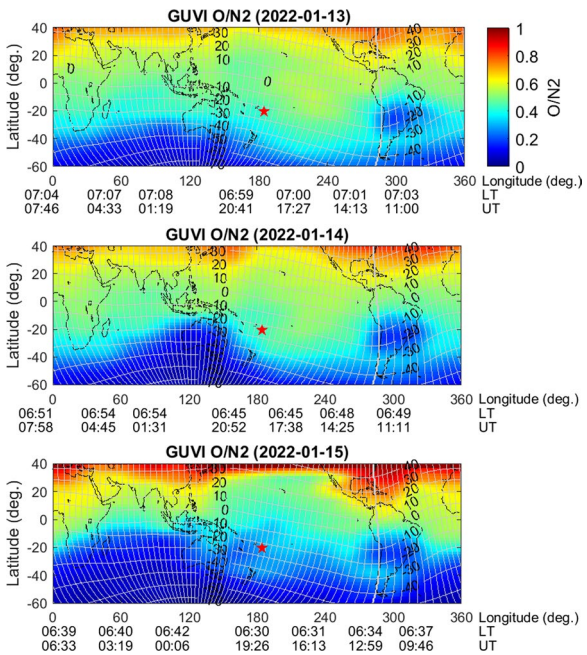


**Fig. 9** Global distribution of GUVI O/N2 ratio on 13–15 January 2022. The gray curves are the magnetic latitude and longitude grid lines. The red star indicates Tonga's location

as usual, but on the 15th, it decreased noticeably with magnetic latitude. Astafyeva et al. (2022) suggested that the Tonga ionospheric hole is more strongly sustained by the storm effect. However, geomagnetic storms the day before the eruption did not appear to have significantly affected the O/N2 ratio near Tonga. He et al. (2022) modeled the thermosphere O/N2 ratio using TIEGCM, and found that the O/N2-depleted region was more affected by volcanic eruptions. The depletion of the O/N2 ratio over the southern Pacific on January 15 was likely due to the effects of volcanic eruptions rather than storms. This may also have contributed to the long-lasting giant ionospheric depletion.

It is noted that the in situ satellite measurements of ion density show that the EIA trough was accompanied by nighttime plasma bubbles, unlike those density holes observed near Tonga. The equatorial region enters nightside at the onset of a volcanic eruption. The dayside ionospheric hole in the equatorial region exhibits smooth density without substructures (C2E2 and C2E5 of Fig. 2e). After sunset, plasma bubbles are observed within the large depletion region (Fig. 3f and k). However, the ionospheric hole signatures observed near Tonga do not show any strong irregularities (Fig. 3l and m). Intense plasma bubbles reaching magnetic latitudes of 35°N were observed in the Asia–Pacific region (100–160°E) (Rajesh et al. 2022), whereas no bubbles appeared in Tonga (magnetic latitudes of 30°S). Rajesh et al. (2022) suggested that the Lamb and gravity waves generated by the volcano propagated out away from Tonga and met the sharp plasma density gradient to trigger intense plasma bubbles. The reason that such stronger bubbles were not seen over Tonga might be that these conditions are not satisfied during the sunset period.

The ICON detected the sharp increase in plasma density at both boundaries of the ionospheric hole (Fig. 2f and k). The reduced O/N2 ratio can cause the structure of ionospheric holes by decreasing plasma density in the EIA crest region. However, this cannot explain the plasma density enhancements in the boundaries. The Tonga volcano may induce strong upward plasma drift. As the EIA structure is lifted up due to upward E×B drift, the plasma can diffuse down along the geomagnetic field lines and away from the equator. When the F7/C2 and ICON pass through this structure, two satellites detected intense perpendicular drift (Fig. 10e, j, o) in the EIA trough depletion. Moreover, the field-aligned drifts of the northern and southern hemispheres are northward (Fig. 10d) and southward (Fig. 10i), respectively, and consequently away from the magnetic equator. The two sharp peaks at the boundary of the ionospheric hole indicate the E×B effect drift by intense prereversal enhancement (PRE). Rajesh et al. (2022) reported such intense PRE

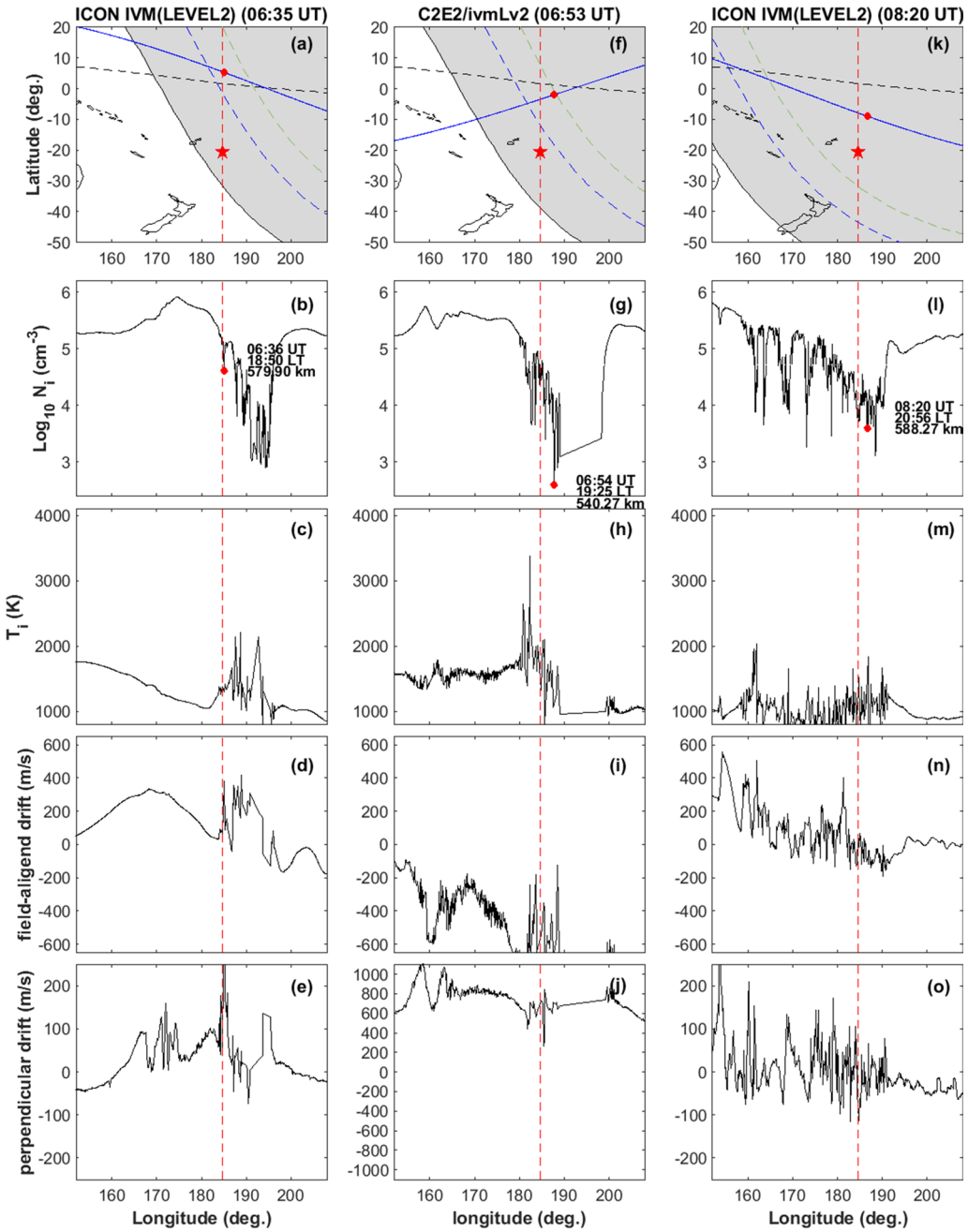


**Fig. 10** Same as Fig. 6 but within the EIA trough

on January 15, 2022, even though it was during the solstice period. They suggested that combining the Lamb-wave effect over the equator and the weakened EIA crests driven by the magnetic storm may cause the very intense PRE. The intensification of PRE is contributed by the combined effects of the storm time disturbances and composition changes during the recovery phase, which weakened the EIA at daytime and resulted in sharper electron density gradient. They explain that the weakened EIA crest enabled efficient zonal circulation, and the wind over the EIA region plays a crucial role in enhancing the PRE. This, together with the perturbations resulting from the volcano eruption yielded the unusually intense PRE. The much more intensified northern EIA around 0630 UT in Fig. 5 is the result of the intensified PRE. The enhanced PRE produced a deep equatorial

trough (Fig. 5), and the extended region of the depleted plasma density progressively appears over the equatorial regions expanding to western longitudes with sunset. The Tonga ionosphere hole subsequently evolves over to the southern EIA crest latitude, diminishing the effects of PRE over this region after 0530 UT (Fig. 5). Note that the southern hemisphere EIA crests were already weakened due to the effects of the magnetic storm (c.f., Rajesh et al. 2022). Moreover, the IVM measurements after 0511 UT indicate that the plasma transport resulting from the volcano induced perturbations was predominantly poleward in the later hours (Fig. 3). Eventually, the two depleted regions almost overlap, with a very narrow separation between them in the GIS map. The sketch in Fig. 8 illustrates the merging of the EIA trough depletion with the depleted region near Tonga, leading to the giant ionosphere hole. Note that the sketch only provides a meridional view of the impact of the enhanced PRE indicated by the arrows, and the bird view of the GIS map illustrates the resulting electron density distribution in the evening period. Eventually, the depth of the ionosphere hole near Tonga is almost identical to that of the EIA trough (C2E5 of Fig. 2m, Swarm of Fig. 2n).

The Tonga volcanic eruption also injected a large amount of water vapor into the thermosphere, affecting the UV emissions observed by DMSP F-16/SSUSI over Tonga (Paxton et al., 2022).This may have a scenario similar to the ionospheric holes resulting from rocket launches (Bernhardt et al. 2001; Chou et al. 2018; Lin et al. 2014; 2017a, b; Liu et al. 2018; Park et al. 2016; 2022b), due to the recombination of ionospheric oxygen ions and water molecules in the rocket exhaust, which reduces the oxygen ion and electron densities. The water vapor induced photochemical processes likely resulted in the absorption of the thermospheric emissions at different wavelengths, such as 121.6 nm, 135.6 nm and 130.4 nm (not shown here), causing a decrease in their intensities. Thus, the large amount of water vapor due to the Tonga volcanic eruption might also be partly responsible for the creation of a strong and long-lasting ionospheric hole.

## Conclusions

In this study, we have investigated the evolution of the giant ionospheric hole during the 2022 Tonga volcanic eruption using TEC, F7/C2, ICON, Swarm, and GIS observations. The giant ionospheric hole extended over a wide region of 160°-200°E and 25°S-20°N and lasted for about 11 h (05–16 UT). The main findings can be summarized as follows:

1. The ionospheric hole near Tonga strongly expanded southward due to strong poleward drift along the magnetic field lines. A deep EIA trough emerged above the magnetic equator due to the intense upward drift observed by F7/C2 and ICON.
2. The simultaneous observations showed that the ionosphere hole near Tonga combined itself with the EIA trough and finally evolved into the giant ionosphere hole around 07 UT.
3. The plasma inside the ionospheric hole had an enhancement of temperature, strong perturbation of field-aligned drift and perpendicular drift. The ionospheric hole was accompanied by thermospheric neutral density depletion.
4. The impulsive pressure by successive eruptions, trans-equatorial wind, O/N2 depletion, and water vapor injection into high altitude were suggested as possible factors that contributed to the huge and long-lasting ionosphere hole after Tonga volcanic eruption.

To understand the mechanism of this unprecedented ionospheric hole by Tonga volcanic eruption, it is necessary to perform a modeling study on how the strong successive impulses and interhemispheric wind change the motion and density of the ionospheric plasma.

#### Acknowledgements

We thank TASA, NOAA and UCAR for operation and data handling of FORMOSAT-7/COSMIC-2.

#### Author contributions

JMC conducted data analysis and wrote the first draft of the manuscript. CCL designed this study and helped the interpretation of the results. PKR supported the F7/C2 GIS data analysis and interpreted the results. JTL provides sunset terminator data. MC interpreted the results. YSK contributed to the interpretation of the results. SPC managed the F7/C2 satellite data and helped the data analysis. All authors read and approved the final manuscript.

#### Funding

This work was supported in part by the National Science and Technology Council under 112-2811-M-006-025 and 112-2111-M-006 -005 and Taiwan Space Agency under NSPO-S-111517 and TASA-S-1120057.

#### Availability of data and materials

The F7/C2 IVM and GIS data are available at the Taiwan Analysis Center for COSMIC (TACC, https://tacc.cwb.gov.tw/v2/download.html) or the UCAR COSMIC Data Analysis and Archive Center (CDAAC, http://cdaac-www.cosmic.ucar.edu). The TEC data are accessible from the Geological hazard information for New Zealand (GeoNet, https://www.geonet.org.nz/data/types/geodetic) and the Geoscience Australia GNSS data archive (https://www.ga.gov.au/scientific-topics/positioning-navigation/geodesy/gnss-networks). The ICON IVM data can be downloaded from https://icon.ssl.berkeley.edu/Data. Swarm data are available at https://swarmdiss.eo.esa.int/#swarm. The TIMED/GUVI data are available at http://guvitimed.jhuapl.edu/data_products. The GRACE-FO data are available at the Delft University of Technology's thermosphere database (http://thermosphere.tudelft.nl).

## Declarations

#### Competing interests

The authors declare that they have no competing interests.

**Author details**
[1]Department of Earth Sciences, National Cheng Kung University, Tainan, Taiwan. [2]Korea Astronomy and Space Science Institute, Daejeon, South Korea. [3]University of Science and Technology, Daejeon, South Korea.

Received: 31 March 2023 Accepted: 9 November 2023
Published online: 08 December 2023

**References**

Aa E, Zhang SR, Erickson PJ, Vierinen J, Coster AJ, Goncharenko LP (2022) Significant ionospheric hole and equatorial plasma bubbles after the 2022a Tonga volcano eruption. Space Weather. https://doi.org/10.1029/2022SW003101

Adam D (2022) Tonga volcano eruption created puzzling ripples in Earth's atmosphere. Nature 601:497. https://doi.org/10.1038/d41586-022-00127-1

Afraimovich EL, Astafyeva EI, Demyanov VV et al (2013) A review of GPS/GLONASS studies of the ionospheric response to natural and anthropogenic processes and phenomena. J Space Weather Space Clim 3:A27. https://doi.org/10.1051/swsc2013049

Amores A, Monserrat S, Marcos M, Argüeso D, Villalonga J, Jordà G, Gomis D (2022) Numerical simulation of atmospheric Lamb waves generated by the 2022 Hunga-Tonga volcanic eruption. Geophys Res Lett 49:e2022GL098240. https://doi.org/10.1029/2022GL098240

Astafyeva E (2019) Ionospheric detection of natural hazards. Rev Geophys 57:1265–1288. https://doi.org/10.1029/2019RG000668

Astafyeva EI, Afraimovich EL (2006) Long-distance propagation of traveling ionospheric disturbances caused by the great Sumatra-Andaman earthquake on 26 December 2004. Earth Planets Space 58:1025–1031

Astafyeva E, Maletckii B, Mikesell TD, Munaibari E, Ravanelli M, Coisson P, Manta F, Rolland L (2022) The 15 January 2022 Hunga Tonga eruption history as inferred from ionospheric observations. Geophys Res Lett 49:e2022GL098827. https://doi.org/10.1029/2022GL098827

Bates S, Carlowicz M (2022) Tonga volcano plume reached the mesosphere. NASA Earth Observatory. https://earthobservatory.nasa.gov/images/149474/tonga-volcanoplume-reached-the-mesosphere. (Accessed 17 February 2022)

Bencze P, Almár I, Illés-Almár E (2000) Further results referring to the neutral density depletions attributed to plasma bubbles. J Atmos Sol Terr Phys 62:1339–1350. https://doi.org/10.1016/S1364-6826(00)00149-8

Bernhardt PA, Huba JD, Kudeki E, Woodman RF, Condori L, Villanueva F (2001) Lifetime of a depression in the plasma density over Jicamarca produced by space shuttle exhaust in the ionosphere. Radio Sci 36(5):1209–1220. https://doi.org/10.1029/2000RS002434

Chen C-H, Tsai H-F, Wang L-Y, Lin C-HC, Liu J-Y, Yeh W-H (2021) The comparison of topmost radio occultation electron densities with in-situ ion densities from FORMOSAT-7/COSMIC-2. Terr Atmos Ocean Sci 32:953–958. https://doi.org/10.3319/TAO.2021.07.26.01

Chou MY, Lin CH, Yue J, Chang LC, Tsai HF, Chen CH (2017a) Medium-scale traveling ionospheric disturbances triggered by Super Typhoon Nepartak (2016). Geophys Res Lett 44:7569–7577. https://doi.org/10.1002/2017GL073961

Chou MY, Lin CCH, Yue J, Tsai HF, Sun YY, Liu JY, Chen CH (2017b) Concentric traveling ionosphere disturbances triggered by Super Typhoon Meranti (2016). Geophys Res Lett 44:1219–1226. https://doi.org/10.1002/2016GL072205

Chou MY, Shen MH, Lin CCH, Yue J, Chen CH, Liu JY, Lin JT (2018) Gigantic circular shock acoustic waves in the ionosphere triggered by the launch of FORMOSAT-5 satellite. Space Weather 16:172–184. https://doi.org/10.1002/2017SW001738

Chou M-Y, Braun JJ, Wu Q, Heelis RA, Zakharenkova I, Cherniak I, Pedatella NM, Stoneback RA (2021) Validation of FORMOSAT-7/COSMIC2 IVM ion density and TGRS orbit electron density. Terr Atmos Ocean Sci 32:939–951. https://doi.org/10.3319/TAO.2021.06.22.01

Christensen AB et al (2003) Initial observations with the Global Ultraviolet Imager (GUVI) on the NASA TIMED satellite mission. J Geophys Res 108(A12):1451. https://doi.org/10.1029/2003JA009918

Dautermann T, Calais E, Lognonné P, Mattioli GS (2009a) Lithosphere– atmosphere–ionosphere coupling after the 2003 explosive eruption of the Soufriere Hills Volcano. Montserrat Geophys J Int 179:1537–1546. https://doi.org/10.1111/j.1365-246X.2009.04390.x

Dautermann T, Calais E, Mattioli GS (2009b) Global positioning system detection and energy estimation of the ionospheric wave caused by the 13 July 2003 explosion of the Soufriere Hills Volcano. Montserrat J Geophys Res 114:B02202. https://doi.org/10.1029/2008JB005722

Fuller-Rowell TJ, Codrescu MV, Rishbeth H, Moffett RJ, Quegan S (1996) On the seasonal response of the thermosphere and ionosphere to geomagnetic storms. J Geophys Res 101(A2):2343–2353. https://doi.org/10.1029/95JA01614

Global Volcanism Program (2022) Report on Hunga Tonga-Hunga Ha'apai (Tonga). In: Sennert, S.K. (Ed.), Weekly Volcanic Activity Report. Smithsonian Institution and US Geological Survey 12 January-18 January 2022

Gusman AR, Roger J (2022) Hunga Tonga-Hunga Ha'apai volcano induced sea level oscillations and tsunami simulations. GNS Science Webpage. https://doi.org/10.21420/DYKJ-RK41

Harding BJ, Wu Y-JJ, Alken P, Yamazaki Y, Triplett CC, Immel TJ, Gasque CG, Mende SB, Xiong C (2022) Impacts of the January 2022 Tonga volcanic eruption on the ionospheric dynamo: ICON-MIGHTI and Swarm observations of extreme neutral winds and currents. Geophys Res Lett 49:e2022GL098577. https://doi.org/10.1029/2022GL098577

He J, Astafyeva E, Yue X, Ding F, Maletckii B (2023) The giant ionospheric depletion on 15 January 2022 around the Hunga Tonga-Hunga Ha'apai volcanic eruption. J Geophys Res Space Phys 128:e20220JA30984. https://doi.org/10.1029/2022JA030984

Heelis RA, Stoneback RA, Perdue MD, Depew MD, Morgan WA, Mankey MW et al (2017) Ion velocity measurements for the ionospheric connections explorer. Space Sci Rev 212:615–629. https://doi.org/10.1007/s11214-017-0383-3

Heki K (2006) Explosion energy of the 2004 eruption of the Asama Volcano, central Japan, inferred from ionospheric disturbances. Geophys Res Lett 33:L14303. https://doi.org/10.1029/2006GL026249

Heki K, Ping J (2005) Directivity and apparent velocity of coseismic ionospheric disturbances observed with a dense GPS array. Earth Planet Sci Lett 236:845–855. https://doi.org/10.1016/j.epsl.2005.06.010

Heki K, Otsuka Y, Choosakul N, Hemmakorn N, Komolmis T, Maruyama T (2006) Detection of ruptures of Andaman fault segments in the 2004 Great Sumatra Earthquake with coseismic ionospheric disturbances. J Geophys Res 111:B09313. https://doi.org/10.1029/2005JB004202

Huba JD, Joyce G, Krall J, Fedder J (2009) Ion and electron temperature evolution during equatorial spread F. Geophys Res Lett 36:15102. https://doi.org/10.1029/2009GL038872

Illés-Almár E, Almár I, Bencze P (1998) Neutral density depletions attributed to plasma bubbles. J Geophys Res 103:4115–4116. https://doi.org/10.1029/97JA02963

Immel TJ, England SL, Mende SB, Heelis RA, Englert CR, Edelstein J, Sirk MM (2018) The ionospheric connection explorer mission: Mission goals and design. Space Sci Rev 214(1):13. https://doi.org/10.1007/s11214-017-0449-2

Kakinami Y, Kamogawa M, Tanioka Y, Watanabe S, Gusman AR, Liu J, Watanabe Y, Mogi T (2012) Tsunamigenic ionospheric hole. Geophys Res Lett 39:00G27. https://doi.org/10.1029/2011GL050159

Kanai R, Kamogawa M, Nagao T, Smith A, Guillas S (2022) Robust uncertainty quantification of the volume of tsunami ionospheric holes for the 2011 Tohoku-Oki Earthquake: towards low-cost satellite-based tsunami warning systems. Nat Hazard 22(3):849–868. https://doi.org/10.5194/nhess-22-849-2022

Kil H, DeMajistre R, Paxton LJ, Zhang Y (2006a) Nighttime Fregion morphology in the low and middle latitudes seen from DMSP F15 and TIMED/GUVI. J Atmos Sol Terr Phys 68:1672–1681. https://doi.org/10.1016/j.jastp.2006.05.024

Kil H, Paxton LJ, Su SY, Zhang Y, Yeh H (2006b) Characteristics of the storm-induced big bubbles (SIBBs). J Geophys Res 111:A10308. https://doi.org/10.1029/2006JA011743

Kornfeld RP, Arnold BW, Gross MA, Dahya NT, Klipstein WM (2019) GRACE-FO: the gravity recovery and climate experiment follow-on mission. J Spacecraft Rockets 56(3):931–951. https://doi.org/10.2514/1.A34326

Laundal KM, Richmond AD (2017) Magnetic coordinate systems. Space Sci Rev 206:27–59. https://doi.org/10.1007/s11214-016-0275-y

Lin CH (2005) Low-latitude ionosphere variations during magnetic disturbances, PhD dissertation. Natl. Cent. Univ, Chung-li, Taiwan
Lin CH, Lin JT, Chang LC, Liu JY, Chen CH, Chen WH, Huang HH, Liu CH (2012) Observations of global ionospheric responses to the 2009 stratospheric sudden warming event by FORMOSAT-3/COSMIC. J Geophys Res Space Phys. https://doi.org/10.1029/2011ja017230
Lin CH, Lin JT, Chen CH, Liu JY, Sun YY, Kakinami Y, Matsumura M, Chen WH, Liu H, Rau RJ (2014) Ionospheric shock waves triggered by rockets. Annales De Geophysique 32(9):1145–1152. https://doi.org/10.5194/angeo-32-1145-2014
Lin CH, Chen CH, Matsumura M, Lin JT, Kakinami Y (2017a) Observation and simulation of the ionosphere disturbance waves triggered by rocket exhausts. J Geophys Res Space Physics 122:8868–8882. https://doi.org/10.1002/2017JA023951
Lin CY, Matsuo T, Liu JY, Lin CH, Huba JD, Tsai HF, Chen CY (2017b) Data assimilation of ground-based GPS and radio occultation total electron content for global ionospheric specification. J Geophys Res Space Phys 122:10876–10886. https://doi.org/10.1002/2017JA024185
Lin CY, Lin CCH, Liu JY, Rajesh PK, Matsuo T, Chou MY, Tsai HF, Yeh WH (2020) The early results and validation of FORMOSAT-7/COSMIC-2 space weather products: Global ionospheric specification and Ne-aided Abel electron density profile. J Geophys Res Space Phys 125:1–12. https://doi.org/10.1029/2020JA028028
Lin JT, Rajesh PK, Lin CCH, Chou MY, Liu JY, Yue J, Hsiao TY, Tsai HF, Chao HM, Kung MM (2022) Rapid conjugate appearance of the giant ionospheric Lamb wave signatures in the Northern Hemisphere after HungaTonga volcano eruptions. Geophys Res Lett 49:e2022GL098222. https://doi.org/10.1029/2022GL098222
Liu CH, Klostermeyer J, Yeh KC, Jones TB, Robinson T, Holt O et al (1982) Global dynamic responses of the atmosphere to the eruption of Mount St. Helens on May 18, 1980. J Geophys Res 87(8):6281–6290. https://doi.org/10.1029/ja087ia08p06281
Liu JY, Tsai HF, Jung TK (1996) Total electron content obtained by using the Global Positioning System. Terres Atmos Oceanic Sci 7(1):107–117. https://doi.org/10.3319/TAO.1996.7.1.107(A)
Liu JY, Tsai YB, Chen SW, Lee CP, Chen YC, Yen HY, Chang WY, Liu C (2006a) Giant ionospheric disturbances excited by the M9.3 Sumatra earthquake of 26 December 2004. Geophys Res Lett 33:02103. https://doi.org/10.1029/2005GL023963
Liu JY, Tsai YB, Ma KF, Chen YI, Tsai HF, Lin CH, Kamogawa M, Lee CP (2006b) Ionospheric GPS total electron content (TEC) disturbances triggered by the 26 December 2004 Indian Ocean tsunami. J Geophys Res 111:A05303. https://doi.org/10.1029/2005JA011200
Liu JY, Tsai HF, Lin CH, Kamogawa M, Chen YI, Lin CH, Huang BS, Yu SB, Yeh YH (2010) Coseismic ionospheric disturbances triggered by the Chi-Chi earthquake. J Geophys Res 115:A08303. https://doi.org/10.1029/2009JA014943
Liu JY, Chen CH, Lin CH, Tsai HF, Chen CH, Kamogawa M (2011) Ionospheric disturbances triggered by the 11 March 2011 M90 Tohoku earthquake. J Geophys Res 116:A06319. https://doi.org/10.1029/2011JA016761
Liu JY, Chen CH, Sun YY, Chen CH, Tsai HF, Yen HY, Chum J, Lastovicka J, Yang QS, Chen WS, Wen S (2016) The vertical propagation of disturbances triggered by seismic waves of the 11 March 2011 M 9.0 Tohoku earthquake over Taiwan. Geophys Res Lett 43:1759–1765. https://doi.org/10.1002/2015gl067487
Liu H, Ding F, Yue X, Zhao B, Song Q, Wan W, Ning B, Zhang K (2018) Depletion and traveling ionospheric disturbances generated by two launches of China's Long March 4B rocket. J Geophys Res Space Phys 123:10319–10330. https://doi.org/10.1029/2018JA026096
Lühr H, Xiong C (2010) IRI-2007 model overestimates electron density during the 23/24 solar minimum. Geophys Res Lett 37:23101. https://doi.org/10.1029/2010GL045430
Lühr H, Park J, Gjerloev JW, Rauberg J, Michaelis I, Merayo JMG, Brauer P (2015) Field-aligned currents' scale analysis per-formed with the Swarm constellation. Geophys Res Lett 42:1–8. https://doi.org/10.1002/2014GL062453
Nakashima Y, Heki K, Takeo A, Cahyadi MN, Aditiya A, Yoshizawa K (2016) Atmospheric resonant oscillations by the 2014 eruption of the Kelud volcano, Indonesia, observed with the ionospheric total electron contents and seismic signals. Earth Planet Sci Lett 434:112–116. https://doi.org/10.1016/j.epsl.2015.11.029
Olsen N, Friis-christensen E, Floberghagen R et al (2013) The Swarm satellite constellation application and research facility (SCARF) and Swarm data products. Earth Planets Space 65:1189–1200. https://doi.org/10.5047/eps.2013.07.001
Otsuka Y, Kotake N, Tsugawa T, Shiokawa K, Ogawa T, Effendy S, Saito M, Kawamura T, Maruyama NH, Komolmis T (2006) GPS detection of total electron content variations over Indonesia and Thailand following the 26 December 2004 earthquake. Earth Planet Space 58:159–165. https://doi.org/10.1186/BF03353373
Park J, Kil H, Stolle C, Lühr H, Coley WR, Coster A, Kwak YS (2016) Daytime midlatitude plasma depletions observed by Swarm: Topside signatures of the rocket exhaust. Geophys Res Lett 43:1802–1809. https://doi.org/10.1002/2016GL067810
Park J, Heelis R, Chao CK (2021) Ion velocity and temperature variation around topside nighttime irregularities: contrast between low-and mid-latitude regions. J Geophys Res Space Phys 126(2):e2020JA028810. https://doi.org/10.1029/2020JA028810
Park J, Huang CS, Eastes RW, Coster AJ (2022a) Temporal evolution of low-latitude plasma blobs identified from multiple measurements: ICON, GOLD, and Madrigal TEC. J Geophys Res Space Phys 127:e2021JA029992. https://doi.org/10.1029/2021JA029992
Park J, Rajesh PK, Ivarsen MF, Lin CCH, Eastes RW, Chao CK, Coster AJ, Clausen L, Burchill JK (2022b) Coordinated observations of rocket exhaust depletion: GOLD, Madrigal TEC, and multiple low-Earth-orbit satellites. J Geophys Res Space Phys 127:e2021JA029909. https://doi.org/10.1029/2021JA029909
Paxton LJ et al (1999) Global ultraviolet imager (GUVI): measuring composition and energy inputs for the NASA Thermosphere Ionosphere Mesosphere Energetics and Dynamics (TIMED) mission, SPIE Opt. Spectrosc Tech Instrum Atmos Space Res 3756:265
Paxton LJ et al (2004) GUVI: A hyperspectral imager for geospace. Proc SPIE Int Soc Opt Eng 5660:227–240. https://doi.org/10.1117/12.579171
Paxton LJ, Schaefer R, Wolven B, Zhang Y, Kil H (2022, December 14). Observations of the Hunga-Tonga Eruption by TIMED/GUVI and DMSP SSUSI instruments. American Geophysical Union (2022) (AGU 2022), Chicago, IL. USA Zenodo. https://doi.org/10.5281/zenodo.7510242
Rajesh PK, Lin CCH, Lin JT, Lin CY, Liu JY, Matsuo T, Huang CY, Chou MY, Yue J, Nishioka M, Jin H, Choi JM, Chen SP, Chou M, Tasi HF (2022) Extreme poleward expanding super plasma bubbles over Asia-Pacific region triggered by Tonga volcano eruption during the recovery-phase of geomagnetic storm. Geophys Res Lett 49:e2022GL099798. https://doi.org/10.1029/2022GL099798
Richmond AD (1995) Ionospheric electrodynamics using magnetic apex coordinates. J Geomag Geoelectr. https://doi.org/10.5636/jgg.47.191
Saito A, Tsugawa T, Otsuka Y, Nishioka M, Iyemori T, Matsumura M, Saito S, Chen CH, Goi Y, Choosakul N (2011) Acoustic resonance and plasma depletion detected by GPS total electron content observation after the 2011 off the Pacific coast of Tohoku Earthquake. Earth Planet Space 63:863–867. https://doi.org/10.5047/eps.2011.06.034
Shinagawa H, Iyemori T, Saito S, Maruyama T (2007) A numerical simulation of ionospheric and atmospheric variations associated with the Sumatra earthquake on December 26, 2004. Earth Planets Space 59:1015–1026. https://doi.org/10.1186/BF03352042
Shinagawa H, Tsugawa T, Matsumura M, Iyemori T, Saito A, Maruyama T, Jin H, Nishioka M, Otsuka Y (2013) Two-dimensional simulation of ionospheric variations in the vicinity of the epicenter of the Tohoku-oki earthquake on 11 March 2011. Geophys Res Lett 40:5009–5013. https://doi.org/10.1002/2013GL057627
Shults K, Astafyeva E, Adourian S (2016) Ionospheric detection and localization of volcano eruptions on the example of the April 2015 Calbuco events. J Geophys Res 121:10303–10315. https://doi.org/10.1002/2016JA023382
Su SY, Chao CK, Yeh HC, Heelis RA (2003) Observations of shock impact, disturbance dynamo effect, and a midlatitude large-density depletion at 600 km altitude on the 17 April 2002 storm day. J Geophys Res 108:1310. https://doi.org/10.1029/2002JA009752
Sun YY, Liu JY, Lin CY, Tsai HF, Chang LC, Chen CY, Chen CH (2016) Ionospheric F2 region perturbed by the 25 April 2015 Nepal earthquake. J Geophys Res Space Physics 121:5778–5784. https://doi.org/10.1002/2015JA022280
Themens DR, Watson C, Zagar N, Vasylkevych S, Elvidge S, McCaffrey A, Prikryl P, Reid B, Wood A, Jayachandran PT (2022) Global propagation of ionospheric disturbances associated with the 2022 Tonga volcanic eruption.

Geophys Res Lett 49:e202GL098158. https://doi.org/10.1029/2022GL098158
Tsugawa T, Saito A, Otsuka Y, Nishioka M, Maruyama T, Kato H, Nagatsuma T, Murata KT (2011) Ionospheric disturbances detected by GPS total electron content observation after the 2011 off the Pacific coast of Tohoku Earthquake. Earth Planet Space. https://doi.org/10.5047/eps.2011.06.035
Woodman RF, La Hoz C (1976) Radar observations of F region equatorial irregularities. J Geophys Res 81(31):5447–5466. https://doi.org/10.1029/ja081i031p05447
Wright CJ, Neil Hindley M, Alexander J et al (2022) Tonga eruption triggered waves propagating globally from surface to edge of space. ESS Open Arch. https://doi.org/10.1002/essoar.10510674.1
Xiong C, Park J, Lühr H, Stolle C, Ma SY (2010) Comparing plasma bubble occurrence rates at CHAMP and GRACE altitudes during high and low solar activity. Ann Geophys 28:1647–1658. https://doi.org/10.5194/angeo-28-1647-2010
Zettergren MD, Snively JB (2015) Ionospheric response to infrasonic-acoustic waves generated by natural hazard events. J Geophys Res Space Phys 120:8002–8024. https://doi.org/10.1002/2015JA021116
Zettergren MD, Snively JB (2019) Latitude and longitude dependence of ionospheric TEC and magnetic perturbations from infrasonic-acoustic waves generated by strong seismic events. Geophys Res Lett 46:1132–1140. https://doi.org/10.1029/2018GL081569
Zettergren MD, Snively JB, Komjathy A, Verkhoglyadova OP (2017) Nonlinear ionospheric responses to large-amplitude infrasonic-acoustic waves generated by undersea earthquakes. J Geophys Res Space Phys. https://doi.org/10.1002/2016JA023159

## Publisher's Note